

An artificial vision-based control system for automatic heliostat positioning offset correction in a central receiver solar power plant

M. Berenguel^{a,*}, F.R. Rubio^{b,1}, A. Valverde^{c,2}, P.J. Lara^b, M.R. Arahal^b,
E.F. Camacho^b, M. López^b

^a *Departamento de Lenguajes y Computación, Área de Ingeniería de Sistemas y Automática, Universidad de Almería, Carretera Sacramento s/n, E-04120 La Cañada Almería, Spain*

^b *Departamento de Ingeniería de Sistemas y Automática, Escuela Superior de Ingenieros, Universidad de Sevilla, Camino de Los Descubrimientos s/n, E-41092 Sevilla, Spain*

^c *Plataforma Solar de Almería (PSA-CIEMAT), Carretera Senés s/n, E-04200 Tabernas (Almería), P.O. Box 22, Spain*

Received 15 April 2002; received in revised form 2 December 2003; accepted 4 December 2003

Communicated by: Associate Editor Lorin Vant-Hull

Abstract

This paper presents the development of a simplified and automatic heliostat positioning offset correction control system using artificial vision techniques and common CCD devices. The heliostats of a solar power plant reflect solar radiation onto a receiver (in this case, a volumetric receiver) placed at the top of a tower in order to provide a desired energy flux distribution correlated with the coolant flow (in this case air mass flow) through the receiver, usually in an open loop control configuration. There exist error sources that increase the complexity of the control system, some of which are systematic ones, mainly due to tolerances, wrong mirror facets alignment (optical errors), errors due to the approximations made when calculating the solar position, etc., that produce errors (offsets) in the heliostat orientation (aiming point). The approximation adopted in this paper is based on the use of a B/W CCD camera to correct these deviations in an automatic way imitating the same procedure followed by the operators. The obtained images are used to estimate the distance between the sunbeam centroid projected by the heliostats and a target placed on the tower, this distance thus is used for low accuracy offset correction purposes. Basic threshold-based image processing techniques are used for automatic correction.

© 2004 Elsevier Ltd. All rights reserved.

Keywords: Artificial vision techniques; Central receiver systems; Automatic control systems

1. Introduction

This paper focuses on the development of a low accuracy offset correction system tested at the CESA-1 plant at the Plataforma Solar de Almería (South East Spain). Details of the layout of this installation, functional diagram and operational aspects including the aiming point strategy used for the TSA solar air receiver can be found in (García-Martín et al., 1999). The current trend in solar concentrator tracking systems is to use open-loop controllers that compute the direction of the

* Corresponding author. Tel.: +34-950-015-683; fax: +34-950-015-129.

E-mail addresses: beren@ual.es (M. Berenguel), rubio@esi.us.es (F.R. Rubio), antonio.valverde@psa.es (A. Valverde).

¹ Tel.: +34-95-448-7350; fax: +34-95-448-7340

² Tel.: +34-950-387-945; fax: +34-950-365-015

solar vector based on location and time (Blanco-Muriel et al., 2001). When controlling the temperature and flux distribution in the volumetric receiver, the algorithms calculate the amount of the shift using an equation appropriate for each heliostat depending on its current temperature dependent focal length and orientation dependent aberrations in addition to beam errors and sun size. As a first approximation, a heliostat aiming point strategy providing a desired energy flux correlated with the air mass flow through the receiver can be selected to solve the control problem. Nevertheless, there are error sources that increase the complexity of the control system (Stone and Lopez, 1995): time, ephemeris equations (sun model), site location (latitude and longitude), heliostat position in the field, time-varying astigmatism and cosine effects, processor accuracy, atmospheric refraction, control interval and structural, mechanical and installation tolerances. Some of these error sources are systematic ones, mainly due to tolerances (joints, encoder, etc.), wrong mirrors facets alignment (optical errors), errors due to the approximations made when calculating the solar position (Blanco-Muriel et al., 2001), etc. Heliostat beam quality error sources are analysed in (King, 1982).

The approximation adopted in this paper to overcome some of these error sources (mainly those related to the calculation of the solar position and to tolerances) is based on the use of a B/W CCD camera which captures images of the sun reflected by each of the heliostats of the field onto a target devoted to the task of offset correction. The reflection of the light coming from the sun produces a shape that continuously changes due to the sun–earth relative movement. The obtained images serve as feedback information that allows the automatic calculation of the distance between the center of the target and the sunbeam centroid in such a way that this error signal can be used for adjustment purposes. The use of artificial vision algorithms permits the calculation of the center of the target and the sunbeam centroid. After the calculation of the required displacement of the motors of the heliostats (encoder steps), the system sends this information to the central control system (μVAX station) to perform the correction.

There exist several works from the late '70s and early '80s on the Solar One Ten Megawatt Solar Central Receiver Power Plant at Daggett, California in which the fundamental approach presented in this paper was originally developed, not only aimed at compensating offsets of the heliostats but also to characterise total beam power, irradiance distribution, beam centroid, tracking error, overall mirror reflectivity and the sun's radiance distribution, which could be used to compare the actual flux distribution with the theoretical flux distribution for each of the 1818 heliostats, at any time during the day (Stone, 1986; Hallet and Gervais, 1977; King and Arvizu, 1981; King, 1982). The approach was

based on the beam characterization system (BCS) (Thalhammer, 1979; Phipps, 1979; Strachan, 1992; Blackmon, 1984; Blackmon et al., 1999). The BCS, originally termed the digital image radiometer (DIR), was conceived and developed by McDonnell Douglas (now a wholly owned subsidiary of The Boeing Company), and installed at Solar One as part of the DOE/Sandia contract (DE-AC03-798f10499). The Solar One BCS determined the irradiance distribution of the reflected beam from a heliostat on one of four trapezoidal targets mounted below the central receiver. Each of the 1818 heliostats was sequentially moved automatically onto the target such that "image grabs" could be taken with a digitizer, and the centroid of the beam determined and compared with the theoretical position. From this position difference on the target, the tracking error was determined and the heliostat tracking aim point was then corrected, based upon various algorithms. The video camera was modified to provide for background subtraction, control of black-level (which can vary with temperature), elimination of automatic gain control, etc., and to allow its use for various purposes (Blackmon and Edwards, 1990; Blackmon and Stone, 1996; Stone and Blackmon, 1995, 1999). Various algorithms were used to assess and validate data, or discard it and retake the measurements. Factors such as wind speed, mean and standard deviation of the centroid variation, solar irradiance variations, etc., were taken into account. These steps were necessary to have accurate determinations of the net irradiance distribution, and thus accurate corrections for the heliostat tracking. The BCS provided a number of data displays for the plant operators and was capable of operating in both manual and automatic data acquisition modes and it was integrated with the data acquisition system (DAS) and the heliostat array controller (HAC) such that automatic updates of heliostat aimpoint biases could be made and overall heliostat optical performance monitored. Later, Sandia developed a system for use at their test facility in Albuquerque.

These systems are more complete and accurate than that presented in this paper, that is less ambitious and has a different objective than those previously published in the literature in the sense that its objective is simply to replace the operator in the task of performing offset correction and it focuses on the explanation of a software tool that helps the operator to automatically perform the task of offset correction that is currently performed manually in this plant using common CCD cameras without any type of modification. With the developed system tasks like determining the beam flux distribution, beam power and reflector surface flatness or optically characterizing heliostats (like BCS does) cannot be performed. The system tries to imitate the way in which operators perform the offset correction, that is by watching an image on a TV screen obtained from a

typical B/W CCD camera installed in the field and trying to center the centroid of the reflected sun image with the center of a target. That is the reason of why the system presented in this paper only does offset correction based on this simple image obtained from the CCD, without including modifications to the video camera and without using more complex aiming algorithms, as the objective was only to facilitate the operation, relying on the corrections that the aiming point strategy does during nominal operation (that implicitly compensates for tracking errors and low accuracy). The daily operation is based on selecting several groups of heliostats that have to focus reflected solar radiation onto fixed aimpoints defined on the receiver surface (for instance, five aimpoints are defined for CESA-1 operation with TSA configuration). The selection of these groups is based on theoretical studies to achieve desired flux and temperature distribution in the receiver (this last related to security reasons, as temperature gradients within the receiver must be bounded). During operation, an aimpoint strategy is used to try to achieve the mentioned desired flux and temperature distribution, based on the assumption that the heliostats focus the sun rays on the pre-defined aimpoint. If large offsets exist, more corrections will have to be done by the aimpoint strategy, increasing the complexity of the operation with the system. Thus, the main impact of the corrections on receiver performance is that a smaller number of corrections should be carried out by the aiming point strategy, diminishing the transients that could lead to undesired temperature gradients within the solar receiver. The paper tries to explain different aspects of the developed work as: (i) the technique used to calculate the position of the centroid of the projected image of the sun, (ii) the strategy followed when the offset is such that the centroid lies out of the view field of the camera, (iii) other problems that appear in the application (lens distortion, vibrations in windy days, sun reflections in the tower, etc.), (iv) the software tool used by the operators, etc.

As has been mentioned before, the task of detecting and eliminating the heliostats offsets is performed by operators at the PSA, increasing their workload (this is a time-consuming task) and consuming hours that cannot be devoted to nominal operation, as the offsets have to be corrected under the same conditions (daylight). If high accuracy is required, some corrections should be performed during each day due to time-dependent drift (Mancini, 1999). After the work of (Blanco-Muriel et al., 2001), the aiming algorithms are being changed at PSA and smaller aiming errors are being obtained, thus decreasing the frequency of offset correction tasks. The development and implementation of an automatic closed loop control system using images captured by the CCD camera to perform the automatic offsets correction became an important issue, allowing the operator to be

kept out of this task and only performing the supervision of the control results.

The paper is organized as follows: in Section 2, a brief description of the offset correction problem is given. Section 3 is devoted to describing the visual feedback-based control system. In Section 4, the development and implementation of the offset adjustment algorithm is explained. Section 5 presents some results of the application. Finally, some conclusions are given in Section 6.

2. The offset correction problem

The problem that the systematic errors produce in the operation of the solar plant is manifested in a deviation of the projected sun shape, which can be far from the expected point. Each heliostat has a pre-defined aimpoint to which it has to point at the beginning of the operation. As is pointed out in (Stone, 1986), the offset correction problem consists in comparing the actual sunbeam centroid position on a target to a command reference position to determine the error in the sunbeam centroid location. The sunbeam centroid position error is then analysed to correlate the error to errors in the heliostats' track alignment system. In other works referenced in the introduction, a digital image radiometer evaluates the heliostat by measuring the total beam power, irradiance distribution, beam centroid, tracking accuracy and overall mirror reflectivity. New coefficients are established for the heliostats' track alignment system to automatically correct for errors in the system, this eliminates the need for resurveying and field work normally associated with aligning heliostats. In the alignment program, calculations are made for the sun's position based upon the stored time data when the measurements were made. Such factors as the sun's azimuth and elevation are calculated. The program then calculates the orientation of the heliostat based upon the sun's position and the command position of the sunbeam. Once the program has calculated the optimum heliostat position, this information is compared with the stored measurements made. In the error transformation routine errors between the command position and the measured positions are used to calculate the alignment error coefficients. The aimpoint errors are corrected by changing the database stored values.

In the application shown in this paper, a target placed below the volumetric receiver of the CESA-1 plant (Fig. 1) is used to test the accuracy of the heliostats positioning typically once a week to assure a correct and safe operation. In order to do so, a B/W CCD camera (equipped with a pan-tilt mechanism and with an automatic contrast/brightness adaptation mechanism) is used by an operator who modifies the azimuth and elevation coordinates (encoder steps) of the heliostat by a

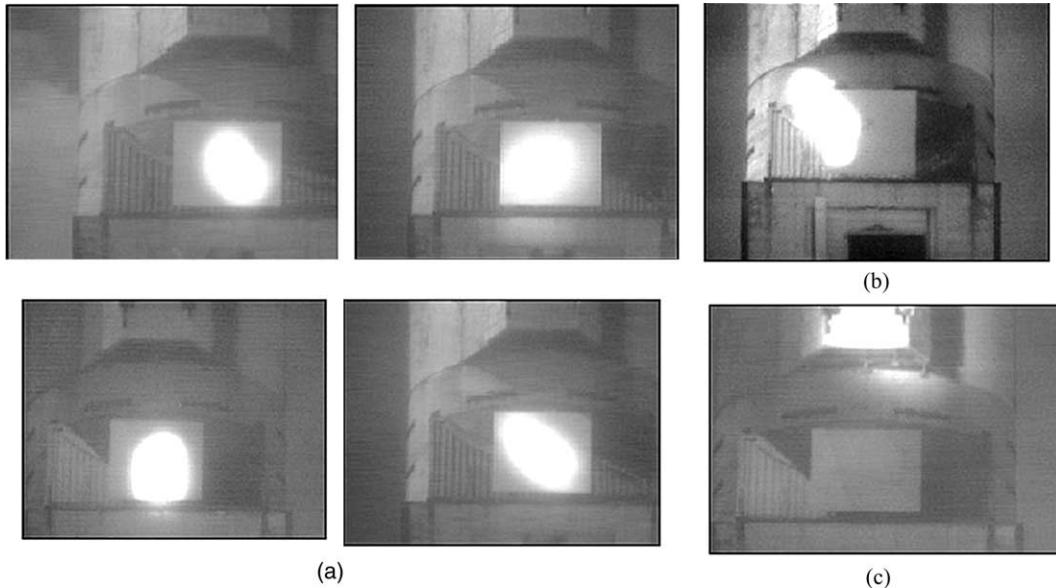


Fig. 1. Details of the target and different shapes of the image of the sun projected by the heliostats: (a) centered ellipsoids (the shape orientation changes during the day), (b,c) ellipsoids out of the target due to aiming errors.

trial and error procedure till the sunbeam centroid coincides with the center of the target. The commands are sent by the operator using different programs implemented in a μVAX station, that processes these control actions and sends the appropriate signals to the local controllers (microprocessors) of the servomotors to move the heliostats to the positions indicated by the control program. The system can also be used during operation, as one heliostat can be deviated from its spot to correct its offset in real time. In the applications in which these corrections are manually performed, it is impossible or quite expensive to carry out this correction during operation, as more than one operator should be needed. In the next section, the developed automated system for offset compensation is explained.

3. Artificial vision-based control system

Fig. 2 shows a scheme of the architecture of the offset correction system. An existing B/W CCD camera was connected to a frame-grabber (Imagination PXC200) with PCI bus for real time transmission of images into memory that was installed in the computer, allowing the capture of images with resolution 640×480 (NTSC) and 768×576 (PAL/SECAM). All the stages of the developed system have been embedded within a user-friendly software tool. This tool has been developed using Visual C++, allowing the development of standard Windows-type interfaces, device-independent programs and the use of pre-installed code. The corrective actions are

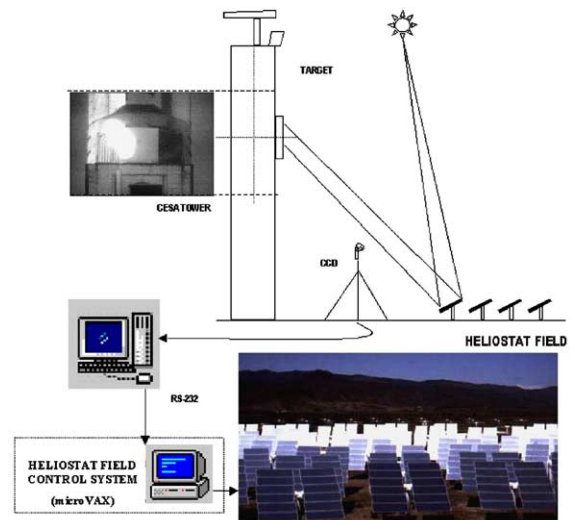


Fig. 2. Diagram of the offset compensation system.

generated in this PC and are finally sent to the μVAX via a serial port (see Fig. 2). The μVAX station processes these control actions and sends the appropriate signals to the local controllers of the servomotors to move the heliostats to the positions indicated by the control program.

The implementation of the automatic control system allows the simplification and optimisation in the operation, as the control program developed automatically decides the correct control actions, then interrogates the

operator about the proposed correction (optional) and sends the corresponding commands to the μVAX to achieve the desired heliostat movements.

4. Development and implementation of the offset adjustment algorithm

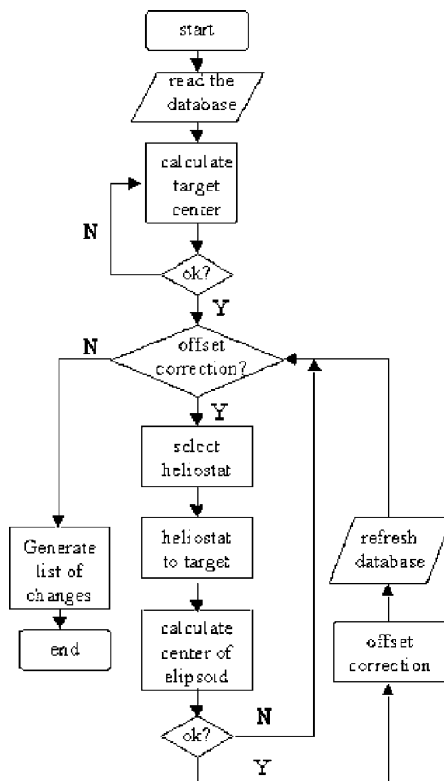
4.1. Reading the database

The movement of the heliostats is discrete (resolution limited by the encoders). The database of the central controller contains, for each one of the 300 heliostats of the field, the following information: row and column (position in the field), $(XYZ)_{hel}$ heliostat center of rotation related to the base of the tower, kind of heliostat (heliostats from different manufacturers are currently in use), nominal elevation and azimuth angles in encoder step units and related information not relevant for the purpose of offset compensation. The encoder resolution is limited to $\pi/4096$ rad. The nominal angles are used in the solar vector calculation in such a way that, in an ideal situation, the heliostats should aim at a target placed on the tower at the beginning of the operation. Notice that due to the discrete nature of the movement of the motors, it is impossible to *exactly* correct the

deviations. The process followed to correct the offset is shown in Fig. 3.

4.2. Calculation of the center of the target

As the CCD camera is used for different purposes, the operator should manually adjust its position (by remotely acting on pan-tilt motors) in such a way that the captured image can show the target. The algorithm that calculates the center of the target is based on threshold detection techniques in such a way that in a first stage, the grey-level of the points belonging to the target are determined. To facilitate this task, the algorithm makes use of the fact that the target should be centered (with some tolerances) in the image (as this is done by the operators acting on the cursors placed at the operation room). First, the image of the target without illumination from the heliostats is captured and the histogram (number of pixels *vs.* grey-level intensity) of a portion of this image is calculated (using values of a rectangle around the center of the image). Once the most representative grey-level intensity of the pixels in the selected rectangle has been obtained, two thresholds are defined to distinguish those pixels belonging to the target (intensity between both thresholds) from those of its environment. The selection of two thresholds is



1. Read the database.
2. Target image capture
3. Calculate the target centre
4. Select heliostat (automatically or manually)
- iterative process*
5. Sun projected shape image capture
6. Calculate the shape centroid
7. Calculate the shaft encoders displacements to be sent to the heliostat, both in azimuth and elevation coordinates in order to minimise the distance between the centre of the target and the reflected shape centroid.
8. Refresh database (shadow database) and generate a list of changes to inform the central control system of the changes performed.

Fig. 3. Flow diagram of the offset correction problem.

necessary due to the fact that the segments of the target do not produce the same intensity colour (grey-level), mainly due to mechanical and mounting distortions and also due to the fact that only a part of the target is being used for threshold selection purposes. These thresholds (TH1 and TH2) are selected to be near the peak with the maximum value of grey intensity (grey_max) in the histogram: low TH1 = grey_max - SHIFT, high TH2 = grey_max + SHIFT. The amount of SHIFT (30) has been heuristically obtained by a trial and error procedure using different experiments in different operating conditions (different illumination levels) and thus is not a general recommendation, as it depends on the camera settings. The reason for using a fixed SHIFT instead of exploring the histogram is due to the fact that if the target is not adequately centered, it is possible to obtain pixels with many different intensity levels, producing a wide threshold that leads to errors in the discrimination of the target. Fig. 4 shows one of the obtained histograms (many of them have been obtained) under hard operating conditions (early in the morning with the sun far from the solar midday).

In a second step the central row of the target is calculated, that is, the horizontal line crossing the center of the target. The same applies to the central column.

These processes are calculated simultaneously to the application of the threshold detection algorithm (the resulting image is shown in Fig. 4(c)). The steps followed in the calculation of the central row and column were (Fig. 5):

(1) Taking into account the size of the image (576 × 768 pixels), in a first step a vertical scan is performed taking into account only those pixels belonging to rows over the middle of the image (<576/2) and those belonging to the central column (= 768/2). In this way, a detection of the pixels belonging to this vertical line with grey-level belonging to the threshold interval is performed, starting with the central pixels (bottom-up). The discontinuity border between pixels belonging to the threshold interval and those out of the target is found in this simple way. As the dimensions of the target are known (both in XY coordinates and in pixels—the camera is not provided with any zoom mechanism and the distance between the camera and the target is fixed) and the upper horizontal line has been detected, the horizontal line containing the center of the target can be easily calculated. Notice that this simple algorithm is valid for those cases in which the center of the complete image contains part of the target, which is always true because the camera is manually positioned using the pan-tilt mechanism.

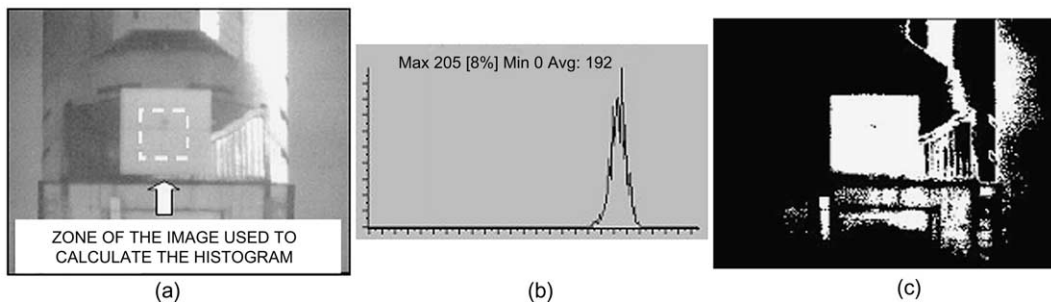


Fig. 4. Example of an image of the target (a), the corresponding histogram (b) and the result of applying the threshold detection algorithm (c).

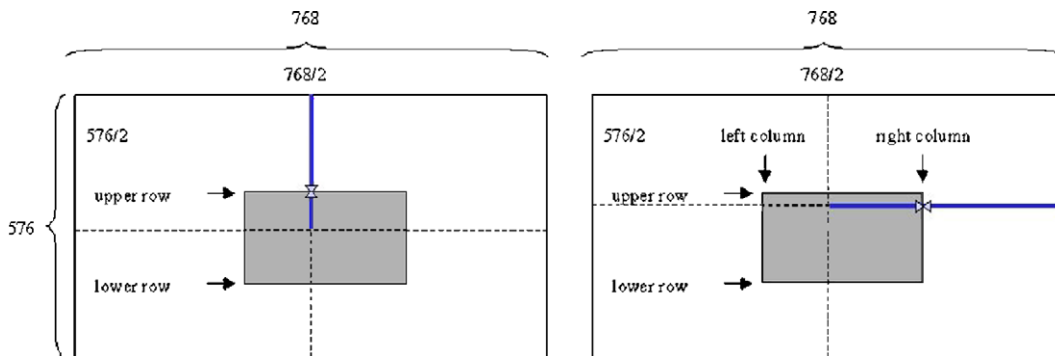


Fig. 5. Simple calculation of the center of the target.

(2) The process followed to calculate the central column of the target is quite similar, but uses the known position of the upper row of the target in such a way that an horizontal line belonging to the image (for instance, 20 rows below the upper one) is selected and is scanned from the center of the image to the right, looking for consecutive pixels belonging to the threshold interval. The central column can thus be obtained knowing the size of the target both in meters and pixels.

(3) The intersection of the central row and column provides the center of target.

Once the center has been calculated, it is shown to the operator in order to test if the calculation is correct. If due to hard operating conditions (mainly producing changes in illumination) the center of the target is not adequately estimated, the operator has only to slightly modify the brightness and contrast of the image using a menu provided in the software tool (see next section).

4.3. Calculation of the sunbeam centroid

The next step consists of sending a heliostat from a standby point to the target (which is pre-defined as an aimpoint, in this case number 9). Fig. 1 shows zones of different images obtained from the CCD camera in which: (a) the heliostat has nearly correct offset coordinates, (b) and (c) the heliostat has wrong offset coordinates. Notice that the intensity of the shape is much higher than that of the other elements in the image, in such a way that the calculation of the sunbeam centroid is simplified using, for instance, threshold detection techniques, as done in the case of the target.

Depending on the selected heliostat, the time elapsed in reaching the target will vary between 18 and 60 s, depending of the kind of heliostat and its position in the field. So, an upper bound of the time the system has to wait till performing the acquisition of a new image is 60 s, this being the first approximation adopted. After several tests, another algorithm was implemented, in such a way that after the first 18 s, each 5 s the center of the centroid was calculated and compared with the previous obtained one (when it appears in the image). When the difference between two consecutive centers was small (less than a small constant selected to take into account the camera vibration due to the wind), the automatic system considered that the heliostat was in its final position. This second algorithm worked well when images were obtained around solar midday. Nevertheless, it did not give good results when direct projections of sun rays impinged on the tower (as happens early in the morning in clear days, e.g. Fig. 4 (a)), before the reflected shape of the sun appeared in the image. Due to the automatic brightness/contrast adaptation mechanism of the CCD, once the reflected shape enters in the view field of the camera, the relative intensity of other sun projections different from the main shape is largely

diminished (e.g. those due to the incidence of sun rays on the side of the tower early in the morning or late in the evening).

Another problem is the case of those heliostats which projection is out of the view field of the camera and do not appear in the captured image. These heliostats are labelled as “*wrong pointing*” ones and their offset can be corrected using a modification of the main algorithm commented later in the paper.

The calculation of the sunbeam centroid was also performed using a threshold detection technique (based on histogram information), as the intensity of the image was near 255. Different more complex image pre-processing algorithms were used, but the added complexity and processing time did not justify their use, because the obtained improvements were not relevant. In order to avoid that other sun projections different from the main one should lead to wrong results, the pixels with intensities over the threshold are grouped according to their intensity level and the existence of neighbours with the same intensity (segmentation). The figure with largest area is selected as that corresponding to the sunbeam shape and its center is calculated. Regarding this criterion of largest area, in the application shown in this work a situation with most of the radiation falling on surfaces that are not essentially perpendicular to the line of sight of the camera does not appear due to the heliostat field—tower—target layout (this has been verified in the tests). In larger plants other criteria should be used, for instance those related with intensity weighting of the image, requiring more sophisticated hardware (cameras, frame grabbers, etc.) that those used in this work.

Fig. 6(a) shows the histogram of the image shown in Fig. 1(b), where the shape of the sun projected by a heliostat can be observed. An intermediate buffer (or auxiliary file) is used to store the different elements of the image. The steps followed in the calculation of the sunbeam centroid were:

(1) Determination of the threshold using the histogram.

(2) Bottom-up/left-right scans are performed comparing each pixel with the threshold, in such a way that if the grey-level of the pixel is below the threshold, it is saved in the auxiliary buffer as a black one (zero intensity). If the intensity of the pixel is greater than the threshold, a fixed intensity value is assigned to it (starting at 255 level) and to all the consequent pixels meeting the threshold condition, until a pixel below the threshold is found (and saved as a black one). The fixed intensity value is decremented and the algorithm continues looking for pixels fulfilling the threshold condition till finding the end of the row. This last processed row is stored into memory, in such a way that the procedure is repeated for the following row, but not only comparing the intensities of the pixels with the

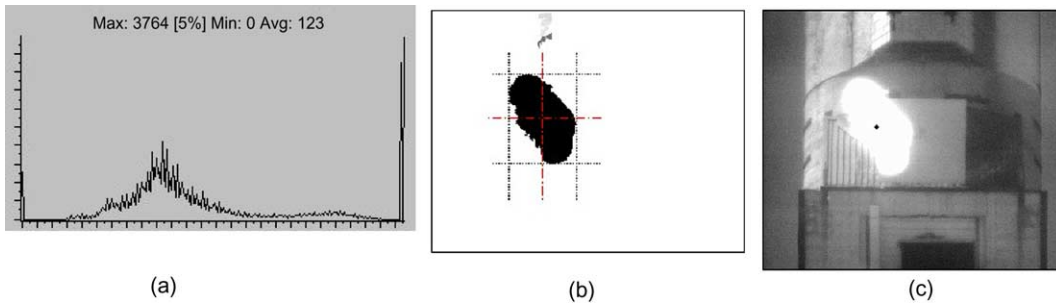


Fig. 6. (a) Histogram used to calculate the sunbeam centroid, (b) result of the application of the segmentation algorithm, (c) shows the centroid position on the real image calculated using (b).

threshold, but also with the intensities of the pixels belonging to the previous processed row, in order to group and label with the same intensity level all the adjacent neighbours (backward modification of the assigned intensity is required in the current processing line to assign the same grey-level to pre-processed ones belonging to the same object in the figure). Fig. 6(b) shows the result (negative image) of the application of the algorithm to the image shown in Fig. 2(b) and (c).

(3) The completely processed rows are stored in an auxiliary buffer, also saving the number of pixels belonging to the used intensities (histogram), in such a way that when the process finishes, the grouped pixels with the predominant intensity should be selected as belonging to the main shape, and the corresponding center will be calculated.

(4) The intermediate buffer is scanned but only looking for pixels with the selected intensity (belonging to the shape after the segmentation process). The extreme pixels (up, low, left and right) are selected and an approximation to the centroid of the figure is obtained by using the center of the outer box including all the pixels of the shape (Fig. 6(b)), using a simple formulae as the intersection of the central column $((\text{right} + \text{left})/2)$ and row of the figure $((\text{up} + \text{low})/2)$.

(5) As is commented in the next section, once the centroid has been calculated, this is indicated in the image shown to the operator, in such a way that the decision of correcting the offsets is done by the operator, depending of the results given by the algorithm. In the mentioned case in which the shape lies out of the view field of the camera, the system returns (0,0) as the sunbeam centroid, and the operator is asked about the inclusion of this heliostat in the group of “wrong pointing” ones, to be corrected with an alternative algorithm.

4.4. Offset correction

The final correction consists in minimising the distance between the center of the target and the sunbeam

centroid. In order to do so, it is necessary to calculate the following data:

- *mm/pixel* relationship: as the camera does not use a zoom mechanism and the dimensions and position of the target are fixed, this is a known relationship. The inclination (Fig. 7) of the target (0.61 rad) and that of the camera (0.35 rad) have been taken into account in this calculation, providing a value of 3700 mm/200 pixels.
- *mm/encoder steps* relationship: this is calculated using the cartesian coordinates of the heliostats related to the base of the tower.

Knowing these values, a relationship can be established between the number of horizontal/vertical pixels in the image corresponding with an azimuth/elevation heliostat movement (encoder steps).

The relationship *mm/encoder steps* varies, not only between heliostats, but depending on the actual elevation and azimuth coordinates of each heliostat. The calculation of this relationship uses the cartesian coordinates of each of the heliostats of the field (X, Y, Z stored in the database) and those of the target in relation to the base of the tower ($X_{\text{target}} = 0, Y_{\text{target}} = 8180, Z_{\text{target}} = 64200$ (mm)). The Z coordinate of the heliostats

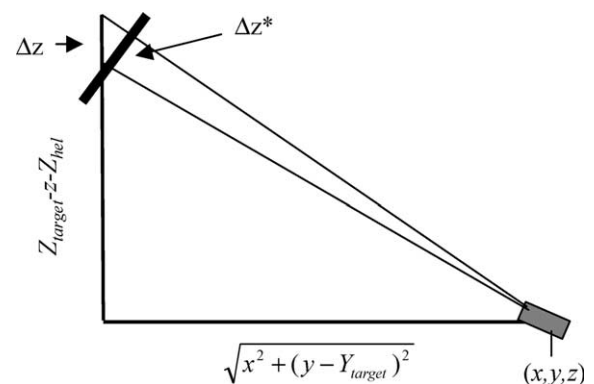


Fig. 7. Approximated calculation of the vertical displacement.

stored in the database has to be augmented with their corresponding height ($Z_{hel} = 3650$ mm).

In what follows, the calculations that the algorithm implements are summarized. It is important to point out that due to the actual architecture of the control system (in which commands can be sent to the μVAX via RS-232 communication, but no information can be received from it, as the main control program installed 20 years ago should be modified), an approximate calculation has to be carried out. The exact calculation could be performed by knowing the azimuth and elevation angles of the heliostats (related to the stow position) in real time when obtaining the solar vector each 4 s (the α angle in Fig. 7 should correspond in this case to the angle measured from the stow position minus $\pi/2$). As no information can be obtained from the μVAX station, the calculations were done based on initial angles stored in a database. The recursivity included in the algorithm helps to correct the errors induced by the approximation.

The steps followed to calculate this relationship are summarized in Table 1. In the left column the approximated calculations used in the algorithm are included. The right column provides the equations that should be used in the case of knowing the azimuth and elevation coordinates of the heliostats in real time, obtained from the calculation of the solar vector. Once these calculations have been performed, the *mm/encoder steps* approximated relationships are obtained both in vertical and horizontal axes. As a simplification to find a trade-off between accuracy and performance, it has been supposed that when an elevation movement is performed, the revolution surface corresponds to a plane and so, its intersection with the plane of the target is a line. In the case of an azimuth movement (maintaining the elevation angle to a fixed value), the revolution surface can be approximated by a cone and its intersection with the plane of the target does not correspond with a horizontal line (in the plane of the target).

Table 1
Offset correction calculations

Approximated calculation	Exact calculation
<i>Vertical axis</i>	
1. Calculation of the angle between the heliostat and the center of the target $tg\alpha = \frac{Z_{target} - z - Z_{hel}}{\sqrt{x^2 + (y - Y_{target})^2}} \Rightarrow \alpha$	1. The Z coordinate of the point of the target to which a heliostat points for an elevation angle a is calculated $tg\alpha = \frac{Z_{target} - z - Z_{hel}}{\sqrt{x^2 + (y - Y_{target})^2}} \Rightarrow \alpha$
2. Add to the calculated angle the increment corresponding to an encoder step. Obtain the height corresponding to the new angle α' $\alpha' = \alpha + \frac{\pi}{4096} \left(\sqrt{x^2 + (y - Y_{target})^2} \right) \cdot tg\alpha'$ $= Z_{target} - z' - Z_{hel} \Rightarrow z'$	2. The point $z + \Delta z$ in the target corresponding to a heliostat elevation angle of $\alpha + \pi/4096$ is calculated (corresponding to a encoder step). $tg\left(\alpha + \frac{\pi}{4096}\right) = \frac{z + \Delta z}{\sqrt{x^2 + (y - Y_{target})^2}} \Rightarrow z + \Delta z$
3. The encoder step indicates a vertical change of the shape corresponding to $\Delta z = z' - z$ in the Z-axis As the target is inclined 0.61 rad, the obtained increment has to be multiplied by $cos(0.61)$ to obtain the real increment related to the plane of the target (Δz^*)	3. By subtracting both quantities the <i>mm/encoder steps</i> relationship can be obtained in the vertical axis (Δz)
<i>Horizontal axis</i>	
1. Calculation of the angle between the heliostat and the center of the target $tg\beta = \frac{x}{\sqrt{(y - Y_{target})^2 + (Z_{target} - z - Z_{hel})^2}} \Rightarrow \beta$	1. The X coordinate of the point of the target to which a heliostat points for an azimuth angle a is calculated $tg\beta = \frac{x}{\sqrt{(y - Y_{target})^2 + (Z_{target} - z - Z_{hel})^2}} \Rightarrow x$
2. Add to the calculated angle the increment corresponding to a encoder step. Obtain the horizontal displacement corresponding to the new angle $\beta' = \beta + \pi/4096$ $\left(\sqrt{(y - Y_{target})^2 + (Z_{target} - z - Z_{hel})^2} \right) \cdot tg\beta' = x' \Rightarrow x'$	2. The point $x + \Delta x$ in the target corresponding to a heliostat azimuth angle of $\beta + \pi/4096$ is calculated (corresponding to a encoder step). $tg\left(\beta + \frac{\pi}{4096}\right) = \frac{x + \Delta x}{\sqrt{(y - Y_{target})^2 + (Z_{target} - z - Z_{hel})^2}} \Rightarrow x$
3. The encoder step indicates a horizontal change of the shape corresponding to $\Delta x = x' - x$ in the X-axis	3. By subtracting both quantities the <i>mm/encoder steps</i> relationship can be obtained in the horizontal axis (Δx)

Nevertheless, the error of approximating this movement by a horizontal one is negligible compared to other sources of errors like the discretization of the movement of the heliostats. If a high accuracy is required, the heliostat position, target center, beam on target and sun position are required to compute tracking errors with vector math (e.g. King, 1982). Once the relationship $mm/ pixel$ and $mm/encoder\ steps$ are known (and thus $pixel/encoder\ steps$ relationship), the algorithm to calculate the number of encoder steps is easy to implement and is based on successive approximations, by subsequently calculating the distance in pixels (both in vertical and horizontal axes) between the center of the target and the sunbeam centroid and calculating the required displacement in encoder steps to minimise this distance (as the effect in mm of a encoder step is known from the previous relationships). Notice that consecutive calculations have to be performed each time a encoder step is performed, as the real displacement in mm changes with the angle of the heliostat, as has been previously mentioned.

Once the number of encoder steps both in elevation and azimuth have been calculated, the system tests the effects of these actions, as accumulated errors in the calculations (approximations done in the $mm/encoder$

$steps$ relationships) and the discrete nature of the control signal can lead to the need of further adjustments, selected by the operator. The performed tests shown that a maximum of three steps are needed in extreme cases. Fig. 8 shows a flow diagram of the complete process.

4.5. Refresh database

Once the offset correction has been calculated, the following command (change heliostat CH) is sent to the μVAX : CH $ffcc, az_offset-AZ, el_offset-EL$, where cc is the characteristic number of the selected heliostat, az_offset and el_offset are the nominal values of azimuth and elevation coordinates of the heliostat, AZ and EL are the corrections that have to be performed. Notice that values of az_offset and el_offset are contained in the central database. A command (BD) also exists to allow the modification of the database with the new values of elevation and azimuth (requires the operator's authorization).

4.6. Wrong pointing heliostats

The correction of the offset of heliostats for which the reflected sun shape does not appear in the view field of

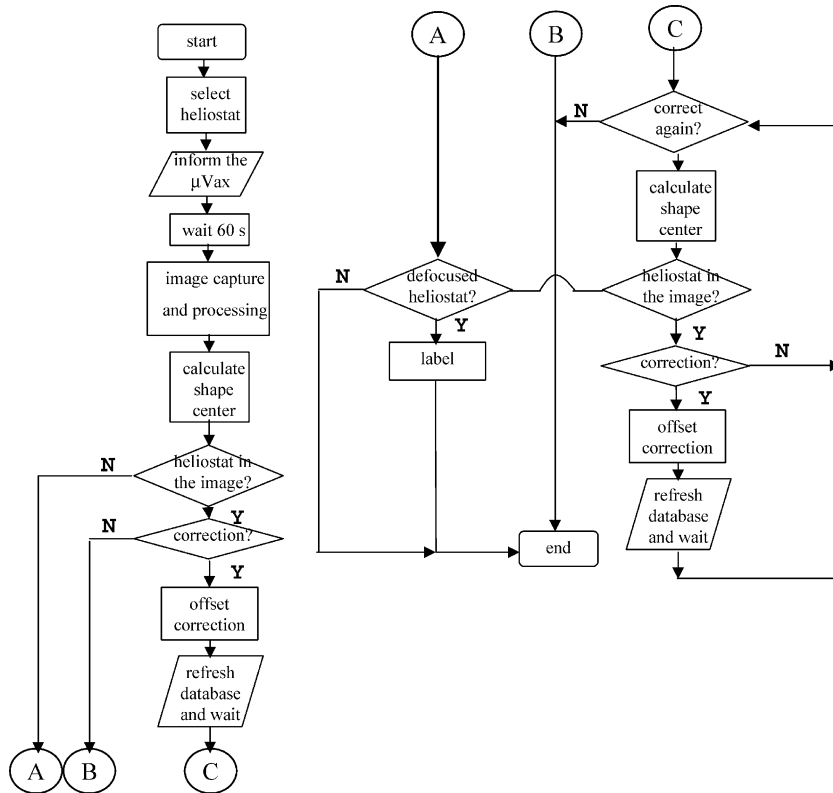


Fig. 8. Flow diagram of the offset correction mechanism.

the image requires the modification of the previous algorithm. Three possible cases are taken into account:

1. The ellipsoid does not appear in any of the captured images each 5 s (during 60 s).
2. Only one image of the shape has been obtained in the intermediate captures.
3. Some images of the shape have been obtained in the intermediate captures.

In the first case, the search is started at an arbitrary zone of the eight neighbour zones defined with the same size of the frame captured by the camera. In the second and third cases, the zone in which the search may start can be automatically found. Heliostat displacements are thus produced and once the ellipsoid enters the image, the normal procedure for offset correction is applied.

5. Implementation and experimental results

5.1. Software tool

The system has been implemented using a windows-based software tool that allows the operators of the plant to supervise the offset correction task through a user-friendly graphic interface (in Spanish). Fig. 9 shows the main window of the application which is divided into

four sections: (1) devoted to show real time images of the target and the reflected ellipsoid, including different processing stages of the algorithm, (2) zone of the window showing the commands sent to the μVAX , (3) a window showing the main characteristics of the test: heliostat number, azimuth and elevation angles, angle/mm and angle/pixel relationships, etc., (4) results of the processing: center of the target, sunbeam centroid, etc.

5.2. System implementation

Before implementing the system at the real plant, several tests were performed using static images obtained at the plant. After this preliminary phase, the system was installed initiating some kind of problems, the main ones related with:

1. The positioning system of the camera, due to strong fluctuations produced by the wind.
2. Optical errors produced by the camera lens (superposed images due to mechanical problems).
3. Illumination variations due to the sun displacement.
4. The implementation of the correcting system for wrong pointing heliostats.

The first two problems were mainly overcome by the plant personnel by both adjusting the mechanical fit of the camera and calibrating the lens. Nevertheless, a

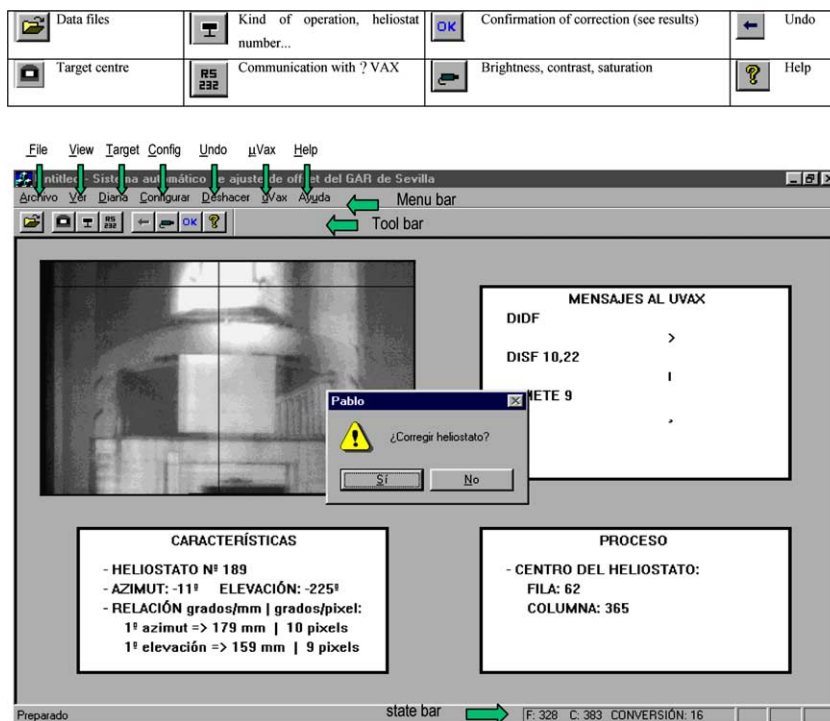


Fig. 9. Software tool.

modification to the software was included to account for these possible error sources. In the first case, the possibility of performing a redundant calculation of the center of the target was included (using different snapshots of that) and in the second case it was noticed that the threshold algorithm discriminated between the real and the superposed image, due to the different intensity levels of both images.

The third problem is due to the sun movement and the direct exposure of the tower to sun rays, changing from the east side near sunrise to the west side near sunset, and lying out of the field of the camera during a significant portion of the operation. Due to this fact, the first version of the algorithm for calculating the sunbeam centroid sometimes provided wrong results when the sun reflection from the tower was visible. This first version did not include the segmentation part explained in Section 4, which was included after noticing this problem thus including two degrees of freedom for determining the real projected sun image (intensity and size).

The fourth source of problems is related to the third one previously commented, due to the fact that the sun reflection can confuse the algorithm when searching for the reflected sun shape each 5 s. So, the modified algorithm was only used in the case of wrong positioning heliostats, waiting 60 s in the standard case to start the processing of the image.

5.3. Tests and results

As a summary of the obtained results with the algorithms explained in this work, Fig. 10(a) shows the differences between the real target center and that calculated by the algorithm in several representative tests. The maximum obtained difference has been 7.4 cm (notice that the target dimensions are 370 cm × 366 cm).

In the case of the sunbeam ellipsoid, Fig. 10(b) contains representative results of 30 tests performed with two heliostats (8,11) (8,12) located in the center of the field (east and west) from 11 to 16 h local time. The largest errors correspond to situations in which the sunbeam centroid is far from the center of the target. As the projected shape approximates the center of the target (as a consequence of the application of the iterative algorithm in less than four steps), the results in the calculations are more precise. It is interesting to mention that in the set of performed test, a percentage of about 90% successful results (similar to those manually obtained by the operators) were obtained when correcting heliostats if the corresponding ellipsoid appears in the image. In the case of “*wrong pointing*” heliostats this percentage of success is about 50% (only two tests have been performed).

6. Conclusions

The development and implementation of an automatic offset correction system for a heliostat field of a solar tower plant has been presented. An algorithm has been developed and tested at the Plataforma Solar de Almería with the help of the head of the operation. Although few tests have been performed (due to the use of the facility in other research programs), the obtained results have been successful. The developed software tool facilitates the task of offset correction to the operators, as they have only to perform the supervision of the process, instead of manually commanding the heliostats. The main reason the offset correction system has been developed is based on the way in which this kind of installation actually operates (see García-Martín et al., 1999) and on safety issues, as temperature gradients within the receiver must be bounded. During

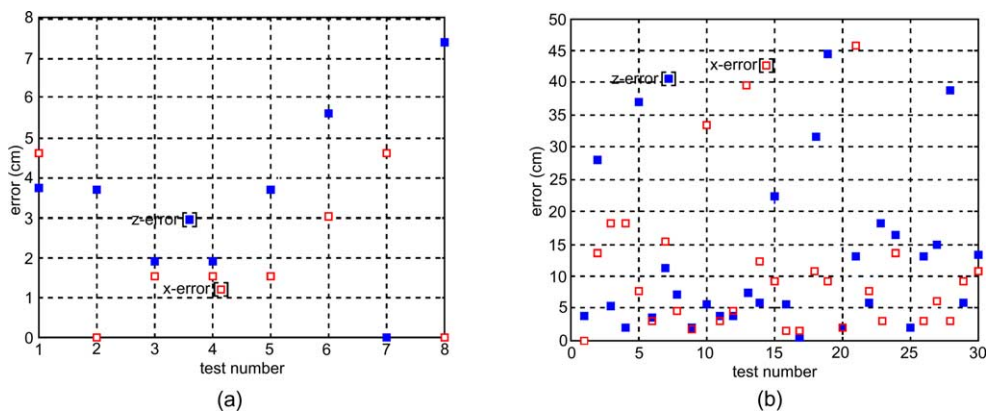


Fig. 10. Representative tests: (a) absolute value of errors in the calculation of the center of the target, (b) the sunbeam centroid. The tests have been performed at different local times during several days.

operation, an aimpoint strategy is used to try to achieve the mentioned desired flux and temperature distribution, based on the assumption that the heliostats focus the sun rays on the pre-defined aimpoint. If large offsets exist, more corrections will have to be done by the aimpoint strategy, increasing the complexity of the operation with the system. Thus, the main impact of the corrections on receiver performance is that fewer corrections should be carried out by the aiming point strategy, diminishing the transients that could lead to undesired temperature gradients within the solar receiver. Regarding the possible application of this kind of system to commercial heliostat fields where operation should be fully automatic, the performed tests show that for small-scale installations the presented algorithms should work well after preliminary tests to determine those parameters obtained by heuristics. For large-scale plants some modifications should probably be required in the direction of the development of more complete and accurate systems, as the BCS developed for Solar One (see references).

Acknowledgements

The authors would like to thank the anonymous reviewers and Dr. Vant-Hull for their suggestions that have helped to improve the manuscript and future works. The authors would also like to thank CICYT for partially funding this work under grants FEDER 1FD99-0957-C02, DPI2001-2380-CO2 and DPI2002-04375-C03. The experiments described in this paper were also performed within the project “Enhancement and Development of Industrial Applications of Solar Energy Technologies”, supported by EEC Program “Human Capital and Mobility—Large Installations Program” and promoted by CIEMAT—Plataforma Solar de Almería, Spain.

References

- Blackmon, J.B., 1984. Development and performance of a digital image radiometer for heliostat evaluation at solar one. In: Proc. of the ASME Solar Engineering Division 6th Annual Conf., Las Vegas, NV, April 8–12.
- Blackmon, J.B., Edwards, D.K., 1990. Apparatus and method for calculation of shape factor, US Patent 4,963,025, October 16.
- Blackmon, J.B., Stone, K.W., 1996. Digital image system for determining relative position and motion of in-flight vehicles, US Patent 5,493,392, February 20.
- Blackmon, J.B., Caraway, M.J., Stone, K.W., 1999. Digital image radiometer applications for solar concentrator optical evaluation. In: Proc. ISES[®] World Congress, Jerusalem, Israel.
- Blanco-Muriel, M., Alarcón-Padilla, D.C., López-Moratalla, T., Lara-Coira, M., 2001. Computing the solar vector. *Solar Energy* 70 (5), 431–441.
- García-Martín, F.J., Berenguel, M., Valverde, A., Camacho, E.F., 1999. Heuristic knowledge-based heliostat field control for the optimization of the temperature distribution in a volumetric receiver. *Solar Energy* 66 (5), 355–369.
- Hallet, R.W., Gervais, R.L., 1977. Central receiver solar thermal power system, vol. III, Book 2, SAN-1108-76-8, MDC G6776, McDonnell Douglas Corp.
- King, D.L., Arvizu, D.E., 1981. Heliostat characterization at the central receiver test facility. *Trans. ASME, J. Solar Energy Eng.* 103, 82–88.
- King, D.L., 1982. Beam quality and tracking accuracy evaluation of second generation and Barstow production heliostats, SAND82-0181, McDonnell Douglas Corp.
- Mancini, T., 1999. Heliostat daily centroid shift, report no. III-1/99. IEA SolarPACES.
- Phipps, G.S., 1979. Heliostat beam characterization system—calibration technique. In: ISA/79 Conf. Proc., Chicago, IL, USA.
- Stone, K.W., 1986. Automatic heliostat track alignment method, US Patent 4,564,275, January 14.
- Stone, K.W., Lopez, C.W., 1995. Evaluation of the solar one track alignment methodology. *Solar Eng. ASME* 1, 521–526.
- Stone, K.W., Blackmon, J.B., 1995. Digital image system and method for determining surface reflective and refractive characteristics of objects, US Patent 5,477,332, December 19.
- Stone, K.W., Blackmon, J.B., 1999. Alignment system and method for dish concentrators, US Patent 5,982,481, November 9.
- Strachan, J.W., 1992. Revisiting the BCS, a measurement system for characterizing the optics of solar collectors. In: 39th Int. Symp. of Instrument Society of America.
- Thalhammer, E.D., 1979. Heliostat beam characterization system—update. In: ISA/79 Conf. Proc., Chicago, IL, USA.